Available online at www.sciencedirect.com
SCIENCE DIRECT®
Journal of Power Sources 134 (2004) 72–79
JOURNAL OF POWER SOURCES
www.elsevier.com/locate/jpowsour

Short communication

Raman spectroscopy of superionic Ti-doped $Li_3Fe_2(PO_4)_3$ and $LiNiPO_4$ structures

G. Butt [a], N. Sammes [b], G. Tompsett [c], A. Smirnova [b,*], O. Yamamoto [d]

[a] *Department of Materials and Process Engineering, University of Waikato, Private Bag 3105, Hamilton, New Zealand*
[b] *Connecticut Global Fuel Cell Centre, University of Connecticut, 44 Weaver Road, Unit 5233, Storrs, CT 06269, USA*
[c] *Department of Chemical Engineering, University of Massachusetts, Amherst, MA 01003, USA*
[d] *Chemistry Department, Mie University 1515, Kamihama, Tsu 514-8507, Japan*

Received 5 January 2004; accepted 26 January 2004

Available online 7 May 2004

Abstract

The Raman spectra of two systems, namely titanium-doped lithium iron and lithium nickel phosphates have been investigated. At room temperature, $Li_3Fe_2(PO_4)_3$ is reported having a monoclinic structure with $P2_1/n$ space group, and transforms to a rhombohedral structure (γ-phase) with *Pcan* space group above 513 K. An orthorhombic structure with *Pnma* space group is reported for $LiNiPO_4$ and Ti-doped $LiNiPO_4$ polycrystalline samples.

The Raman spectra of the first system, specifically $Li_3Fe_2(PO_4)_3$ and Ti-doped $Li_3Fe_2(PO_4)_3$, are assigned with respect to band positions reported in the literature for $Li_3Fe_2(PO_4)_3$ and $Fe_2(SO_4)_3$ and, Nasicon-type compounds $Li_3In_2(PO_4)_3$ and $Na_3Fe_2(PO_4)_3$. Although spectra show a marked change in the broadness and number of bands observed, the overall profile is similar to α-$Li_3Fe_2(PO_4)_3$ which indicates up to 20 mol% solubility of titanium in the $Li_3Fe_2(PO_4)_3$ phase.

The second $LiNiPO_4$ system shows mixed phase behaviour and is composed of orthorhombic $LiNiPO_4$ and a secondary phase, likely a titanium phosphate. With increasing Ti-dopant concentration up to 20 mol%, there is an increase in the relative proportion of the secondary phase, characterised by a strong band at 784 cm^{-1}.

Keywords: Lithium–iron and lithium–nickel phosphates; Raman spectroscopy; Titanium doping; Superconductivity

1. Introduction

Superionic materials possess exceptionally high values of ionic conductivity in the solid state, and have a large number of technological applications including rechargeable lithium batteries, sensors, and displays. They comprise potential to meet the requirements of size-compactness, integration, and stability at ambient temperature, and are desirable for the development of new rechargeable lithium battery systems [1–3].

Lithium-ion oxide conductors have some advantages in practical applications as solid-state electrolytes for batteries. Their advantages include easy synthesis and handling, as well as high decomposition voltage. Typical lithium-ion oxide conductors, such as NASICON-type $LiM_2(PO_4)_3$ (M–Ti, Ge, Zr, Hf) and perovskite-type $Li_{0.5}La_{0.5}TiO_3$ have been widely studied because of their high ionic conductivity. Many of these ionic conductors have titanium as the major component, which can easily take part in lithium intercalation or deintercalation, and sometimes, exhibit appreciable electronic conductivity. However, substitution of the major component with titanium stabilises superionic conductors at room temperature [2].

In this paper, we characterise two systems, namely $Li_3Fe_{2-x}Ti_x(PO_4)_3$, where $x = 0$–0.20, and $Li(Ni_{1-x}Ti_x)PO_4$, where $x = 0$–0.20.

The first system, $Li_3Fe_{2-x}Ti_x(PO_4)_3$, belongs to the $Fe_3(SO_4)_3$-type structure and to the Nasicon family. The structure is based on a three dimensional network of $[Fe_2(PO_4)_3]_x$ of FeO_6-octahedra and PO_4-tetrahedra sharing oxygen vertices. The lithium ions are situated in interstitial voids in the framework [4]. $Li_3Fe_2(PO_4)_3$ has three phases reported [5] namely, monoclinic ($P2_1/n$) α, monoclinic ($P2_1/n$) β and rhombohedral ($R\bar{3}c$) γ. Several

* Corresponding author. Tel.: +1-860-486-8762; fax: +1-860-486-8378.
E-mail address: alevtina@engr.uconn.edu (A. Smirnova).

0378-7753/$ – see front matter © 2004 Elsevier B.V. All rights reserved.
doi:10.1016/j.jpowsour.2004.01.053

Table 1
Raman and infrared modes for the compounds $Na_3Fe_2(PO_4)_3$ and $Li_3Fe_2(PO_4)_3$

Compound	Structure	Space group	Raman active modes (no.)	Infrared active modes (no.)	Acoustic modes	Reference
$Na_3Fe_2(PO_4)_3$	Monoclinic	*C*2/*c* (no. 15) (at 293 K)	$29A_g + 31B_g$ (60)	$32A_u + 34B_u$ (63)	$A_u + 2B_u$	[5]
$Na_3Fe_2(PO_4)_3$	Rhombohedral	$R\bar{3}c$ (no. 167) (at ? K)	$9A_{1g} + 20E_g$ (29)	$11A_{2u} + 21E_u$ (32)	$A_{2u} + E_u$	[5]
α-$Li_3Fe_2(PO_4)_3$	Monoclinic	$P2_1/n$ (no. 14) (at 293 K)	$60A_g + 60B_g$ (120)	$59A_u + 58B_u$ (117)	$A_u + 2B_u$	[3]
γ-$Li_3Fe_2(PO_4)_3$	Orthorhombic	*Pcan* (no. 61) (at 573 K)	$36A_{1g} + 36B_{1g} + 36B_{2g} + 36B_{3g}$ (144)	$35B_{1u} + 35B_{2u} + 35B_{3u}$ (105)	$B_{1u} + B_{2u} + B_{3u}$	[3], this work

workers have utilised Raman and infrared spectroscopy to characterise the structure of the monoclinic $AE_3M_2(PO_4)_3$, where AE = Li and Na, and M = Fe, Sc, In, Zr, Cr [4–11].

Kravchenko et al. [6] have reported the Raman spectrum of $Li_3Fe_2(PO_4)_3$ and $Li_3Sc_2(PO_4)_3$, however, only the bands due to Li vibrations were assessed in any detail and the full assignment of the Raman modes has not been reported to date. Barj et al. [8] report the factor group analysis and spectra of compounds belonging to the Nasicon family of structures, and characterised the short-range disorder occurring in these systems.

The other group of structures studied in this work includes $Li(Ni_{1-x}Ti_x)PO_4$. Abrahams and Easson [12] showed that the main representative of this group, specifically $LiNiPO_4$, has an orthorhombic structure with *Pnma* space group, $a =$

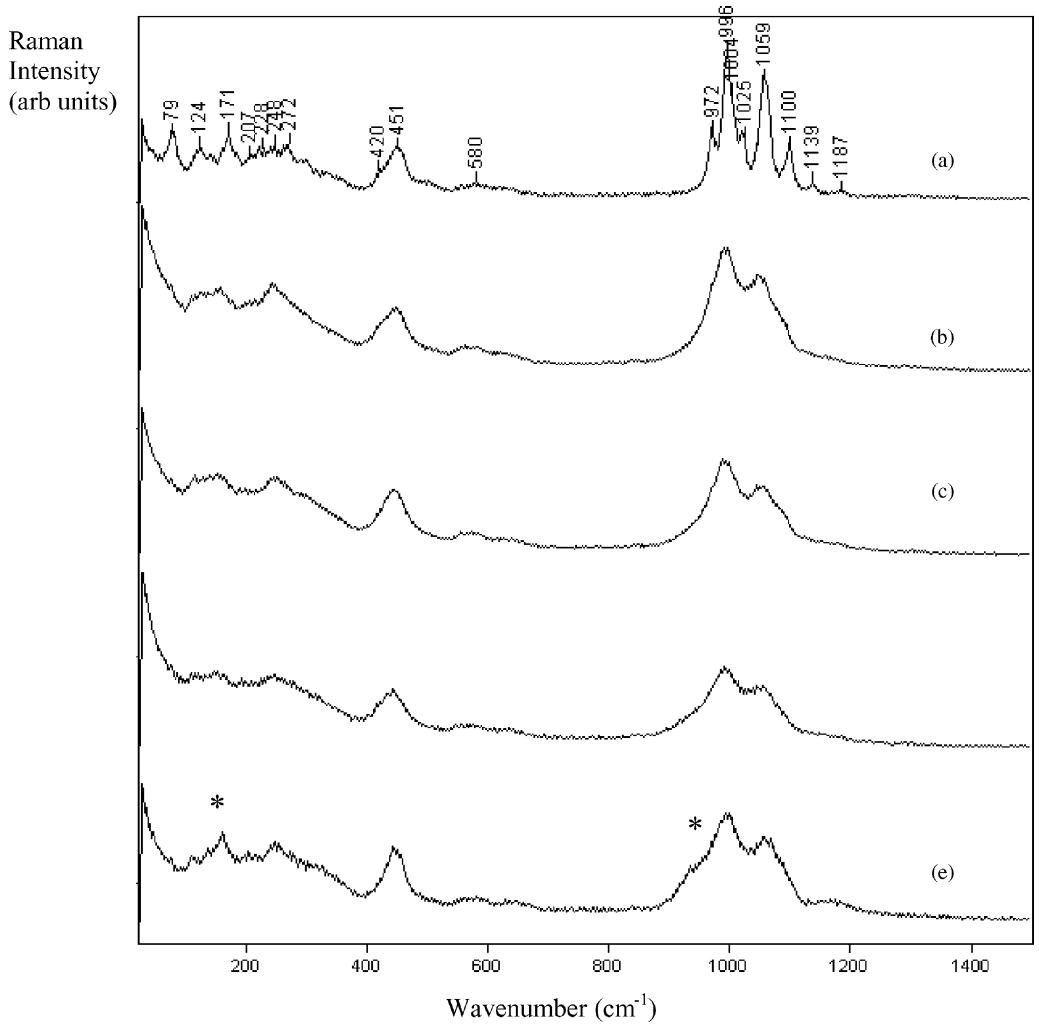

Fig. 1. Raman spectra of $Li_3Fe_{2-x}Ti_x(PO_4)_3$, where $x = 0$ (a), 0.0.5 (b), 0.10 (c), 0.15 (d), and 0.20 (e). Asterisk (*) indicates possible secondary phase.

Table 2
Raman band positions and assignments of $Li_3Fe_2(PO_4)_3$ compared to those observed for isostructural and Nasicon-type structure compounds

$Li_3Fe_2(PO_4)_3$ (this work)	$Li_3Fe_2(PO_4)_3$ [3] (approximately)	$Li_3In_2(PO_4)_3$ [3] (approximately)	$Na_3Fe_2(PO_4)_3$ [5] (approximately)	Assignment [3]
			49 w	Lattice modes
			60 w	Lattice modes
			72 w	Lattice modes
79 m			82 w	Lattice modes
124 w	120		131 m	Lattice modes
141 vw	140	150 vw	147 m	Lattice modes
171 m	160	160 vw	172 m	Lattice modes
186 sh	180		195 m	Lattice modes
207 vw	210	200 m	204 sh	Lattice modes
228 w	220	215 s		Lattice modes
248 w	250	230 s	237 m	Lattice modes
272 w	270	250 s	290 w	Lattice modes
301 w, b	290	300 s		LiO_4, FeO_6 octahedra modes
336 w, b	330	340 s	320 m	LiO_4, FeO_6 octahedra modes
357 w, b	370		330 w	LiO_4, FeO_6 octahedra modes
420 sh	400	410 sh		PO_4 deformations
		425 s		PO_4 deformations
		440 s	445 m	PO_4 deformations
451 m, b	450	450 s		PO_4 deformations
		475 s	480 vw	PO_4 deformations
497 w, b	490	493 sh		PO_4 deformations
		497 m		PO_4 deformations
		500 sh		PO_4 deformations
556 w	530	540 w	543 w	PO_4 deformations
			560 w	PO_4 deformations
580 w, b	590		586 w	PO_4 deformations
			597 w	PO_4 deformations
627 w, b	600		624 w	PO_4 deformations
			642 vw	PO_4 deformations
846 vw				
972 m			963 m	PO_4 vibration of the valency bonds
996 s	990		973 s	PO_4 vibration of the valency bonds
1004 sh	1010		1015 vs	PO_4 vibration of the valency bonds
			1019 sh, s	PO_4 vibration of the valency bonds
1025 m	1020		1025 sh, s	PO_4 vibration of the valency bonds
			1034 sh, s	PO_4 vibration of the valency bonds
1059 s	1050		1045 vs	PO_4 vibration of the valency bonds
1100 m	1090		1060 m	PO_4 vibration of the valency bonds
1139 w	1130		1130 vw	PO_4 vibration of the valency bonds
1187 vw	1180		1180	PO_4 vibration of the valency bonds
	1210			PO_4 vibration of the valency bonds
	1240		1215 m	PO_4 vibration of the valency bonds
1302 vw				

10.0317 Å, $b = 5.8537$ Å, $c = 4.6768$ Å at room temperature. The structure is related to that of olivine, Mg_2SiO_4, with hexagonal closed packed oxygen, with Li and Ni in half the octahedral sites and P in 1/8 of the tetrahedral sites. There exists no previous literature on the Raman spectra of $LiNiPO_4$ or Ti-doped $LiNiPO_4$.

2. Experimental

$Li_3Fe_{2-x}Ti_x(PO_4)_3$, where $x = 0$–0.20, and $Li(Ni_{1-x}Ti_x)PO_4$, where $x = 0$–0.20, were prepared using the standard solid-state technique [13] between Li_3PO_4, Fe_2O_3, TiO_2, NiO, and $NH_4H_2PO_4$. The mixtures with stoichiometric amounts of these materials were ground in an agate mortar. The resulting mixtures were heated in an open crucible at 500 K for 1 h and then at and 900 K for another 1 h to decompose phosphates and nitrates, respectively. This process was followed by further heating at 1100 K for 15 h in air with an intermediate regrinding after 10 h. The final products were quenched to room temperature.

Raman spectroscopy was performed on samples of powders using a Jobin Yvon U 1000 double beam pass spectrometer equipped with a microscope stage for analysing small samples utilising 180° incident geometry. A Spectra

Table 3
Raman band positions of $Li_3Fe_{2-x}Ti_x(PO_4)_3$, where $x = 0$–0.20

0	0.05	0.10	0.15	0.20	$Li_3Fe_2(PO_4)_3$ [3] (approximately)	$Na_3Fe_2(PO_4)_3$ [5] at 670 K
						34
						50
79 m				76 vw		70
124 w	130 m, b	117 m	115 w	112 w	120	122
141 vw	158 m	138 m		138 sh	140	140
171 m		154 m	151 m	161 m	160	
186 sh					180	182
207 vw	213 w	199 vw	194 w	205 w, b	210	
228 w					220	223
248 w	246 m	246 m	247 m, b	245 m, b	250	235
272 w					270	
301 w, b	292 sh	293 sh	281 sh	274 sh	290	
				317 sh		316
336 w, b	345 sh	357 sh			330	
357 w, b					370	
420 sh	427 sh				400	
451 m, b	446 m	444 m	444 m, b	446 m, b	450	446
497 w, b		493 sh		506 vw	490	
556 w	565 w	570 w, b	568 w, b	576 w, b	530	550
580 w, b					590	584
627 w, b	623 w, b	634 w, b	629 w, b	643 w, b	600	616
		788 vw				
846 vw	846 vw	846 vw	845 vw	847 vw		
972 m			938 sh	942 sh		
996 s	994 s	990 s	993 s	996 s	990	
1004 sh		1000 sh			1010	
1025 m					1020	
1059 s	1049 s	1054 s	1054 s	1059 s	1050	1020
1100 m	1083 sh	1081 sh	1084 sh	1082 sh	1090	
1139 w	1124 sh	1128 sh			1130	
1187 vw	1160 vw	1184 vw	1153 vw	1177 w, b	1180	
					1210	
					1240	
1302 vw	1293 vw	1302 vw	1301 vw	1300 vw		

Physics argon-ion laser was employed to excite laser Raman spectra using a 514 nm laser line at an incident power of ca. 10 mW, and a water-cooled photo multiplier tube. Raman spectra were obtained using a 50× objective and 500 μm slit width. The scanning rate used to collect the spectra was kept at 0.5 $cm^{-1}\,s^{-1}$.

3. Results and discussion

3.1. Titanium-doped $Li_3Fe_2(PO_4)_3$ structures

According to [6,10], the space group for the $Na_3Fe_2(PO_4)_3$ has monoclinic $C2/c$ (no. 15) structure with 2 formula units, i.e. $Z = 2$ at room temperature. The monoclinic β-phase is formed (space group, $C2/c$) at 368 K, and above 418K the rhombohedral γ-phase exists ($R\bar{3}c$). Similarly, $Li_3Fe_2(PO_4)_3$ can exist as three structures: low temperature monoclinic ($P2_1/n$) α,β-phase, and high-temperature orthorhombic (*Pcan*). Table 1 shows the Raman and infrared modes for these compounds and structures obtained earlier [6,8] and calculated in this work.

A total of 60 Raman active, 117 infrared active and no coincident or inactive modes were predicted for the low temperature α-phase of $Li_3Fe_2(PO_4)_3$, studied in this work. However, for the high temperature $Li_3Fe_2(PO_4)_3$ γ-phase 144 Raman and 105 infrared modes have been predicted for the orthorhombic structure. The factor group analysis of the $Na_3Fe_2(PO_4)_3$ phases shows the change in the number of active modes with change in symmetry.

The Raman spectra of titanium-doped $Li_3Fe_2(PO_4)_3$ are shown in Fig. 1. The Raman spectrum of $Li_3Fe_2(PO_4)_3$, agrees well with that reported in the literature [5] for the monoclinic α-phase. The band positions are compared in Table 2 with that observed by Kravchenko et al. [6] for $Li_3Fe_2(PO_4)_3$ and those of compounds with similar

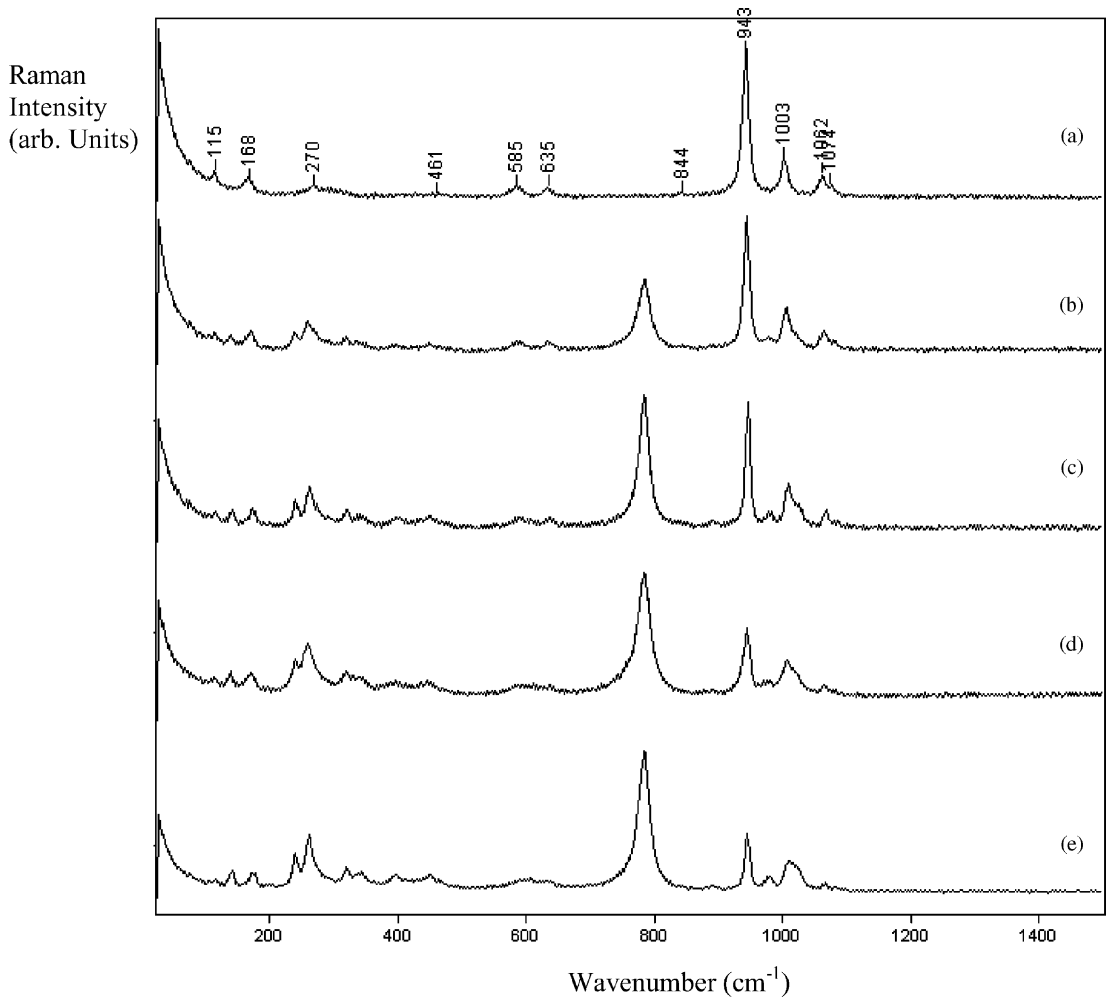

Fig. 2. Raman spectra of $Li(Ni_{1-x}Ti_x)PO_4$, where $x = 0$ (a), 0.05 (b), 0.10 (c), 0.15 (d), and 0.20 (e).

Table 4
Raman band positions of $Li(Ni_{1-x}Ti_x)PO_4$, where $x = 0$–0.20

0	0.05	0.10	0.15	0.20	$LiTi_2(PO_4)_3$ [3]	Assignment [2–4]
			107 vw	108 vw		
115 w	113 w	117 w	115 w	116 w		LNP (lattice)
	139 w	142 w	139 w	141 w	139	*
168 w	163 sh	165 sh				LNP (lattice)
	171 w	175 w	172 w	175 w	177	*
		199 vw	198 vw	201 vw	195	*
	239 w	241 m	242 m	241 m	240	*
270 w	260 m	263 m	260 m	262 m		LNP (lattice)
	273 sh	275 sh	277 sh	276 sh	274	*
		293 vw		291 w		
305 sh						LNP (lattice)
	320 w	322 w	319 w	320 w	310	*
365 vw	342 w, b	345 w, b	343 w	343 w	352	LNP (NiO_6)
		369 vw				
413 w, b	396 w	400 w, b	395 w, b	397 w, b	431	LNP (NiO_6 and PO_4 bending)
461 vw	449 w	450 w, b	447 w, b	450 w, b	448	LNP (NiO_6 and PO_4 bending)
		469 sh		469 sh		
	497 vw					
		534 vw			548	*
585 w	588 w	589 w, b	590 w, b	590 w, b	589	LNP (LiO_6 and PO_4 bending)
				608 w, b		

Table 4 (*Continued*)

0	0.05	0.10	0.15	0.20	$LiTi_2(PO_4)_3$ [3]	Assignment [2–4]
635 w	636 w	639 w	636 w, b	638 w, b	657	LNP (LiO_6 and PO_4 bending)
	785 m	785 s	784 s	785 s	784*	*
844 vw	861 vw	842 vw	853 vw	846 vw		LNP (PO_4 stretching)
		892 vw	891 vw	893 vw		*
943 s	945 s	947 s	947 m	946 m	968	LNP (PO_4 stretching)
	980 w	981 w	978 vw	980 w	987	*
1003 m	1006 m	1009 m	1008 m	1011 m	1006	LNP (PO_4 stretching)
	1023 sh	1014 sh			1016	*
		1027 sh	1025 sh	1025 w		*
1062 m	1063 w	1069 w	1066 w	1067 w	1065	LNP (PO_4 stretching)
1074 w	1081 sh	1084 vw	1084 vw	1082 vw	1093	LNP (PO_4 stretching)
1289 vw	1294 vw	1295 vw				LNP (PO_4 stretching)

vw: very weak; w: weak; m: medium; s: strong; b: broad; sh: shoulder, relative intensity. (∗): secondary phase; LNP: orthorhombic $LiNiPO_4$.

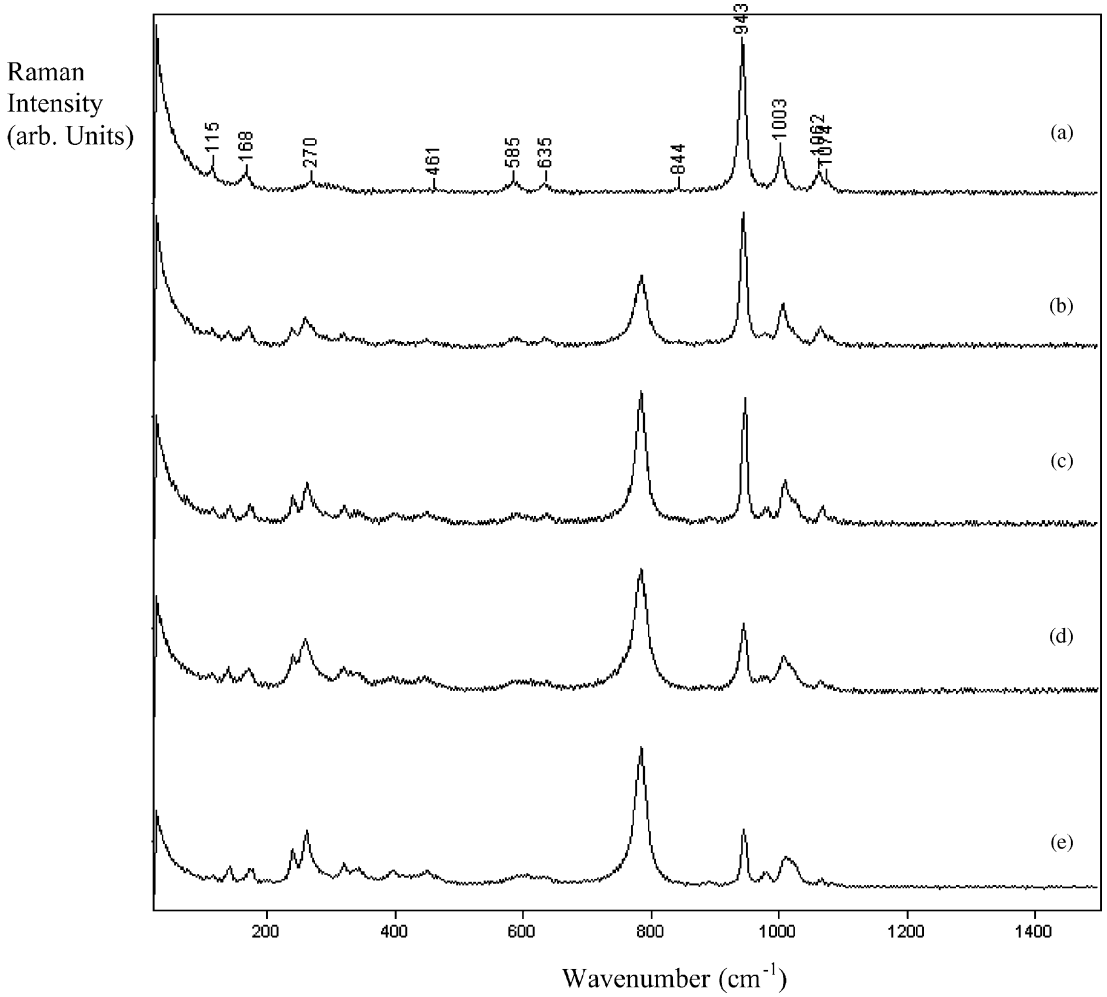

Fig. 3. Raman spectra of $LiNiPO_4$ (a), $Li(Ni_{0.80}Ti_{0.20})PO_4$ (b) and subtraction spectrum of (b)−(a).

structure, to characterise the spectrum. It can be seen that the band position match those reported for $Li_3Fe_2(PO_4)_3$, and the spectra of monoclinic $Li_3In_2(PO_4)_3$ and $Na_3Fe_2(PO_4)_3$ show very similar band positions. The bands are assigned to vibrations, of lattice modes (0–400 cm^{-1}), FeO_6 octahedra (300–400 cm^{-1}), PO_4^{3-} deformations (400–700 cm^{-1}) and vibrations of the valence bonds of PO_4^{3-}, with respect to the work of Kravchenko et al. [6]. A total of 28 bands are observed at room temperature, of the 120 Raman modes predicted for the $P2_1/n$ space group.

The spectra of titanium-doped lithium iron phosphate, $Li_3Fe_{2-x}Ti_x(PO_4)_3$, where $x = 0.05$–0.20, show a Raman profile that is significantly different to that for undoped $Li_3Fe_2(PO_4)_3$. A total of 15 bands are observed, almost half that of the undoped compound, and the bands are broader, particularly in the range 900–1200 cm^{-1}. Table 3 gives a comparison of the band positions of $Li_3Fe_{2-x}Ti_x(PO_4)$ with monoclinic $Li_3Fe_2(PO_4)_3$ and rhombohedral $Na_3Fe_2(PO_4)_3$. The Raman profiles of the Ti-doped $Li_3Fe_2(PO_4)_3$ more closely resembles that of the rhombohedral $Na_3Fe_2(PO_4)_3$ compound. Doping $Li_3Fe_2(PO_4)_3$ with titanium appears to increase the symmetry of the structure likely via the Li^+ ion positions.

At 20 mol% Ti dopant, there are several extra bands observed at 161 and 942 cm^{-1}. These bands may indicate the formation of a secondary phase at the high Ti-dopant level or the formation of a new phase, which is the subject of a present publication.

3.2. Titanium-doped $LiNiPO_4$ structures

The Raman spectra of $Li(Ni_{1-x}Ti_x)PO_4$, $x = 0$–0.20, are shown in Fig. 2. Band positions and relative intensities of the observed spectra are listed in Table 4. For the Raman spectrum of $LiNiPO_4$, there are a total of 15 bands observed at room temperature, of 42 predicted Raman active modes calculated from factor group analysis. The bands are assigned with reference to the relative wave number positions, and compared to the reported assignments of the spectra of $Li_3Fe_2(PO_4)_3$, $LiTi_2(PO_4)_3$, and NiO [6,14,15,16]. The Raman spectra of Ti-doped $LiNiPO_4$ (Fig. 2) show the presence of a secondary phase, characterised by a strong band at 784 cm^{-1}. With increasing Ti-dopant concentration there is an increase in the relative proportion of the secondary phase. Fig. 2 compares of the Raman spectra of $LiNiPO_4$, $Li(Ni_{0.80}Ti_{0.20})PO_4$ and the subtraction spectrum of the two. It can be seen that at 20 mol% Ti, the secondary phase is predominant in the system. The spectrum of the secondary phase (Fig. 3, b−a) matches that of the secondary phase reported by Cretin et al. [15] for the system $Li_{1.3}Al_{0.3}Ti_{1.7}(PO_4)_3$ prepared by the sol gel method, and sintered at 950 °C. Cretin et al. [15] did not assign this secondary phase and reported that it was invisible to X-ray diffraction. It is likely that this secondary phase is a titanium phosphate phase as it increases with increase in Ti-dopant concentration, and the major band at 784 cm^{-1} is within the range for PO_4^{3-} stretching vibrations.

4. Conclusions

The Raman spectra of $Li_3Fe_2(PO_4)_3$ and Ti-doped $Li_3Fe_2(PO_4)_3$ are reported with 28 modes observed of the 120 Raman modes predicted for the monoclinic α-phase of $Li_3Fe_2(PO_4)_3$. The spectra are assigned with respect to band positions reported in the literature for $Li_3Fe_2(PO_4)_3$ and $Fe_2(SO_4)_3$ and Nasicon-type compounds $Li_3In_2(PO_4)_3$ and $Na_3Fe_2(PO_4)_3$. The Raman spectra of $Li_3Fe_2(PO_4)_3$ doped with TiO_2 show a marked change in the broadness and number of bands observed, although the overall profile is similar to $Li_3Fe_2(PO_4)_3$. It has been shown that titanium is soluble in $Li_3Fe_2(PO_4)_3$ up to 20 mol%, however, the Raman spectra resembles that observed for a rhombohedral structure rather than a monoclinic structure.

A total of 15 bands were observed for $LiNiPO_4$ at room temperature, from a total of 42 predicted Raman active modes for the orthorhombic structure with *Pnma* space group. Bands were observed at 115, 168, 270, 305, 365, 413, 461, 585, 635, 844, 943, 1003, 1062, 1074 and 1289 cm^{-1} and assigned to types of vibrations according to the relative wave number positions. Raman spectra of Ti-doped $LiNiPO_4$ show a mixed phase system composed of the orthorhombic $LiNiPO_4$, and a secondary phase, likely a titanium phosphate. With increasing Ti-dopant concentration there is an increase in the relative proportion of the secondary phase, characterised by a strong band at 784 cm^{-1}. Ti is shown to be insoluble in the system $LiNiPO_4$ under these fabrication conditions.

References

[1] M.M. Ahmad, K. Yamada, T. Okuda, Ionic conduction and relaxation in KSn_2F_5 fluoride ion conductor, Physica B 339 (2003) 94–100.
[2] T. Suzuki, K. Yoshida, K. Uematsu, T. Kodama, K. Toda, Z.-G. Ye, M. Ohashi, M. Sato, Structure refinement of lithium ion conductors $Li_3Sc_2(PO_4)_3$ and $Li_{3-2x}(Sc_{1-x}M_x)_2(PO_4)_3$ (M = Ti, Zr) with 0.10 by neutron diffraction, Solid State Ionics 113–115 (1998) 89–96.
[3] H.-C. Freiheit, Order parameter behaviour and thermal hysteresis at the phase transition in the superionic conductor lithium sodium sulphate $LiNaSO_4$, Solid State Commun. 119 (2001) 539–544.
[4] A.K. Padhi, K.S. Nanjundaswamy, C. Masquelier, S. Okada, J.B. Goodenough, Effect of structure on the Fe^{3+}/Fe^{2+} redox couple in iron phosphates, J. Electrochem. Soc. 144 (1997) 1609–1613.
[5] A.B. Bykov, A.P. Chirkin, L.N. Demyanets, S.N. Doronin, E.A. Genkina, A.K. Ivanov-shits, I.P. Kondratyuk, B.A. Maksimov, O.K. Mel'nokov, L.N. Muradyan, V.I. Simonov, V.A. Timofeeva, Superionic conductors $Li_3M_2(PO_4)_3$ (M = Fe, Sc, Cr): synthesis, structure and electrophysical properties, Solid State Ionics 38 (1990) 31–50.
[6] V.V. Kravchenko, V.I. Michailov, S.E. Sigaryov, Some features of vibrational spectra of $Li_3M_2(PO_4)_3$ (M = Sc, Fe) compounds near a superionic phase transition, Solid State Ionics 50 (1992) 19–30.
[7] V.V. Kravchenko, S.E. Sigaryov, Lithium disorder in the vicinity of the superionic phase transition in monoclinic and rhombohedral $Li_3In_2(PO_4)_3$, J. Mater. Sci. 29 (22) (1994) 6004–6010.

[8] M. Barj, G. Lucazeau, C. Delmas, Raman and infrared spectra of some chromium Nasicon-type materials: short-range disorder characterisation, J. Solid State Chem. 100 (1992) 141–150.
[9] S.E. Sigaryov, Fast-ion transport mechanism in $Li_3M_2(PO_4)_3$ crystals (M = Sc, Cr, Fe, In), Mater. Sci. Eng. B13 (1992) 121–123.
[10] V.V. Kravchenko, S.E. Sigaryov, Structural features of the superionic phase transitions in $Na_3Fe_2(PO_4)_3$, Solid State Commun. 83 (1992) 149–152.
[11] M. Barj, H. Perthuis, Ph. Colomban, Relations between sublattice disorder, Solid State Ionics 9/10 (1983) 845–850.
[12] I. Abrahams, K.S. Easson, Structure of lithium nickel phosphate, Acta Cryst. C49 (1993) 925–926.
[13] T. Suzuki, K. Yoshida, K. Uematsu, T. Kodama, K. Toda, Z.-G. Ye, M. Sato, Stabilization of superionic conduction phase in $LiSc_2(PO_4)_3$, Solid State Ionics 104 (1997) 27–33.
[14] V.V. Kravchenko, V.I. Michailov, S.E. Sigaryov, Some features of vibrational spectra of $Li_3M_2(PO_4)_3$ (M = Sc, Fe) compounds near a superionic phase transition, Solid State Ionics 50 (1992) 19–30.
[15] M. Cretin, P. Fabry, L. Abello, Study of $Li_{1+x}Al_xTi_{2-x}(PO_4)_3$ for Li^+ potentiometric sensors, J. Eur. Ceram. Soc. 15 (1995) 1149–1156.
[16] R.E. Dietz, G.I. Parisot, A.E. Meixner, Infrared absorption and Raman scattering processes in NiO, Phys. Rev. B 4 (1971) 2302–2310.